Title

A label-free electrochemical immunosensor based on decorated cellulose nanofibrous membrane for point-of-care diagnosis of amanitin poisoning via human urine

Journal

Lab on a Chip, 23(23)

ISSN

1473-0197

Authors

El-Moghazy, Ahmed Y

Amaly, Noha

Nitin, Nitin

et al.

Publication Date

2023-11-21

DOI

10.1039/d3lc00508a

Peer reviewed

Published in final edited form as:

Lab Chip. ; 23(23): 5009–5017. doi:10.1039/d3lc00508a.

Label-free Electrochemical Immunosensor based on Decorated Cellulose Nanofibrous Membrane for Point-of-Care Diagnosis of Amanitin Poisoning *via* Human Urine

Ahmed Y. El-Moghazy[1,2], **Noha Amaly**[1,2], **Nitin Nitin**[1,3], **Gang Sun**[1]

[1]Department of Biological and Agricultural Engineering, University of California, Davis, CA 95616, USA.

[2]Polymeric Materials Research Department, Advanced Technology and New Materials Research Institute, City of Scientific Research and Technological Applications (SRTA-City), New Borg El-Arab City 21934, Alexandria, Egypt.

[3]Food Science and Technology, University of California, Davis, United States.

Abstract

α-Amanitin (AMN) is one of the deadliest toxins from mushrooms, present in the deadly mushroom species *Amanita phalloides*. It is a bicyclic octapeptide and represents up to 40% of the amatoxins in mushrooms, damaging the livers and kidneys. Current methods of detecting amatoxins are time-consuming and require use of expensive equipment. A novel label-free electrochemical immunosensor was successfully developed for rapid detection of α-amanitin, which was fabricated by immobilization of anti-α-amanitin antibodies onto functionalized cellulose nanofibrous membrane-modified carbon screen-printed electrode. An oxidation peak of the captured amanitin on the tethered antibodies was observed at 0.45 V. The performance of the nanofibrous membrane on the electrode and necessary fabrication steps were investigated by electrochemical impedance spectroscopy (EIS) and cyclic voltammetry (CV). Due to their unique structural features and properties such as high specific surface areas and microporous structure, the nanofibrous membrane as the immunosensor matrix for the antibody tethering exhibited improved electrochemical performance of the electrode by more than 3 times compared with the casted membranes. Under the optimal conditions, the assembled immunosensor exhibited high sensitivity toward α-amanitin detection in the range of 0.009–2 ng mL^{-1} with a limit of detection of 8.3 pg mL^{-1}. The results clearly indicate that the fabricated nanofibers-based-immunosensor is suitable to point-of-care detection of lethal α-amanitin in human urine without any pretreatment within 30 min.

Keywords

α-amanitin; Cellulose; Nanofibers; Electrochemical immunosensor; Point-of-care

Introduction:

Thousands of mushroom poisonings are reported annually around the globe[1–3]. In over 80% of cases of mushroom poisoning, the kind of mushroom is unknown. Based on the poisons

present and the clinical symptoms they cause, toxic mushrooms are frequently categorized[5]. Amatoxins are one of the most toxic groups of mushroom toxins, and are responsible for the majority of fatal mushroom poisonings worldwide. These toxins are produced by several species of mushrooms, including some of the Amanita genus, such as Amanita phalloides, also known as the death cap mushroom, which is responsible for most mushroom poisoning deaths[4].

Amatoxins are highly stable and heat-resistant, which means that they are not destroyed by cooking or processing. Once ingested, they are absorbed rapidly in the small intestine and transported to the liver, where they bind to RNA polymerase II, a critical enzyme involved in protein synthesis. This results in the inhibition of protein synthesis, leading to liver cell death and liver failure[5].

The symptoms of amatoxin poisoning usually appear within 6 to 24 hours after ingestion, and may include gastrointestinal distress (such as nausea, vomiting, and diarrhea), abdominal pain, and dehydration. These symptoms may improve after a few days, but then the patient may develop severe liver damage, which can lead to hepatic encephalopathy, coma, and death. Treatment of amatoxin poisoning often involves supportive care, such as fluid and electrolyte replacement, and sometimes liver transplantation is necessary[6].

The diagnosis of amatoxin poisoning can be challenging, as symptoms may not appear until several hours after ingestion, and may initially resemble a gastrointestinal illness. Currently, there are no rapid or on-site diagnostic tools for amatoxin poisoning, which can delay the diagnosis of poisoning and subsequent treatment[7].

Laboratory-based analysis is typically required, using techniques such as HPLC, mass spectrometry, or ELISA to detect the presence of amatoxins in blood, urine, or mushroom extracts[7,8]. The diagnosis of amatoxin poisoning is usually based on a combination of clinical symptoms, history of mushroom ingestion, and laboratory results. In patients with suspected amatoxin poisoning, treatment should be initiated immediately based on clinical suspicion, even before laboratory results are available[7–9].

Rapid diagnosis of amatoxin poisoning would allow for prompt initiation of appropriate treatment, including the administration of silibinin, which can improve patient outcomes and potentially reduce the need for more invasive treatments such as liver transplantation[9,10]. The development of biosensors for amatoxins is urgently needed to help for the rapid and on-site diagnosis of amatoxin poisoning, which allowing for quick and easy detection of amatoxins in mushroom samples or biological samples from patients with suspected poisoning.

In the recent years, nanomaterials have opened new horizons for the biosensor development with enhanced sensitivity, selectivity, and shortened detection time due to the ultrahigh surface areas[11–15]. Nanofibers (NFs) produced by electrospinning are among the most promising nanomaterials, gained a growing interest during the past decade for a wide range of applications[16–20].The employment of nanofibers with ultrahigh surface area has resulted in sensors with higher sensitivity and lower limits of detection (LOD)[21,22].

In this study, an ultrasensitive label-free electrochemical immunosensor was developed based on citric acid decorated cellulose nanofibrous membranes immobilized with AMN antibodies to rapid detection of AMN in human fluids samples. The membrane is attached onto printed electrodes. Amperometric responses were based on the oxidation of hydroxyindole of the captured AMN molecules on the surface of anti-AMN-modified screen-printed electrodes. The developed label-free electrochemical immunosensor was applied for AMN detection in real human urine samples.

Materials & Methods

Chemicals, Materials, and Instrument.

Cellulose acetate (CA; white powder; Mw = 30,000 Da), N, N-dimethylacetamide (DMAc), citric acid, α-Amanitin were purchased from Sigma (St. Louis, MO). N-Ethyl-N′-(3- dimethyl aminopropyl) carbodiimide hydrochloride (EDC), N-hydroxyl succinimide (NHS), disodium hydrogen phosphate (Na_2HPO_4), and monosodium orthophosphate (NaH_2PO_4) were supplied by Acros Chemical (Pittsburgh, PA, USA). sodium chloride (NaCl), potassium chloride (KCl), bovine serum albumin (BSA), potassium ferricyanide ($K_3[Fe(CN_6)]$), potassium ferrocyanide ($K_2[Fe(CN_6)]$) were purchased from Sigma-Aldrich (Milwaukee, WI, USA), AMN antibody (anti-AMN) was generously donated by Dr. Candace Bever (USDA-ARS). All water used was purified using a Millipore Milli-Q plus water purification system. All chemicals were used as received.

A 263A potentiostat/galvanostat equipped with a frequency response detector (FRD100) (Princeton Applied Research Co., Oak Ridge, TN, USA) was used for the electrochemical measurements. The disposable SPE, comprising a carbon working electrode, a carbon counter electrode, and an Ag/AgCl reference electrode, was purchased from Metrohm USA INC (GA, US). The morphological characterizations of the polymeric nanofibrous membranes were implemented by a FEI 430 Nova NanoSEM scanning electron microscope (SEM).

The FT-IR spectra of membrane materials were achieved by using a Nicolet 6700 spectrometer, following of the pressing of the grounded the Cel-A/Cel NFMs at the different reaction steps with anhydrous KBr, FT-IR spectra of these specimens were scanned in the wavenumber range of 500–4000 cm^{-1} with a resolution of 4 cm^{-1}.

Cellulose nanofibrous membranes production and functionalization:

Cellulose acetate nanofibrous membranes production—Following Fu et al[23]. with minor modifications, cellulose acetate nanofibrous membranes (Cel-A NFMs) were produced through electrospinning. Cellulose acetate was dissolved with vigorous stirring overnight in a solvent combination of DMAC and acetone (1:1 w/w), and solutions of various concentrations (5, 10 and 15 wt%) were prepared. A 10-mL plastic syringe with an 18-gauge tubular metal needle with a flat tip was used for the electrospinning process, which was carried out using a DXES-1 spinning apparatus at a voltage of 20 kV, a distance of 15 cm between the needle tip and the collector surface, and a feeding rate of 1 mL/h for the

delivery of the polymeric solution. The spinning process was performed at room temperature and humidity of 45 ± 5%.

Deacetylation of cellulose acetate nanofibrous membranes—Cellulose nanofibrous membranes (Cel NFMs) were made by deacetylating Cel-A NFMs. To hydrolyze the acetate groups and create Cel NFMs, the deacetylation procedure was carried out in 0.05 M NaOH in 1:1 EtOH/water solutions at room temperature for 48 hours. After rinsing with ultrapure water, the prepared Cel NFMs were dried in a vacuum oven for 12 hours at 80 °C. The acetyl% of the produced cellulose was determined by immersing a membrane sample in 20 mL of 0.05 N NaOH in 50% ethanol for 12 hours at room temperature. Followed by titrating of excess alkali with 0.05 N HCl using a pH meter. The percentage of acetyl % in cellulose was calculated according to equation (1)[24]:

$$\text{Acetyl } \% = (V_B \,.\, C_B - V_A \,.\, C_A)\ 4.3/W \tag{1}$$

Where W is the sample weight, V_B and C_B are the volume and concentration of NaOH solution, and V_A and C_A are the volume and concentration of HCl solution, respectively.

Functionalization of produce nanofibrous membranes—The hydroxyl groups on the Cel NFMs were then reacted with the carboxylic groups of citric acid in a procedure performed as follows[25]: A citric acid solution 8 % (w/v) was prepared in 10 mL of PBS buffer pH 7.2, followed by adding EDC and NHS at a final concentration of 1 mM to the citric acid solution. This mixture was vigorously stirred at room temperature for 2 hours. Then, the Cel NFMs were submerged in the prepared solution for 1 hour at 60 °C. Subsequently, the modified membranes (Cel-CA NFM) were rinsed using PBS and placed in a vacuum oven at 80 °C for 1 h.

AMN Immunosensor fabrication:

Immobilization of anti-amanitin antibodies—Prior to the sensor fabrication, the screen-printed electrodes will be pretreated by applying potentials between 1 and −1.5 V vs. Ag/AgCl in 0.5 M H_2SO_4 until a stable signal is obtained to remove the organic binders. A 4 mm Cel NFM disc with 0.05 mm thickness was laminated on the working electrode of the SPE using a conductive paste to fabricate Cel NFM/SPE, and similarly Cel casted membranes were used for in parallel preparing of Cel CM/SPE. 100 μL of 1mM EDC/NHS was used to activate the carboxylic groups of the Cel-CA NFMs/SPE for 1 hour. After washing with PBS, 10 μL of anti-AMN (100 μg mL^{-1}) antibodies were dropped onto the surface of EDC/NHS decorated Cel-CA NFMs/SPE, and the electrode was kept at 4°C for 1 hour. Followed by being rinsed with PBS to remove any un-immobilized antibodies, the remaining active groups were blocked with 50 μL of 1% BSA for 1 hour at the room temperature, and then rinsed again with PBS. The resulting immunosensor was then operational for AMN detection experiments. The schematic diagram of the assembly steps of the AMN immunosensor and detection mechanism are illustrated in scheme 1.

Electrochemical measurements

The electrochemical characterizations for the assembled immunosensor were performed by cyclic voltammetry and Electrochemical impedance spectroscopy (EIS) in a 2.5 mM ferri/ferrocyanide ($[Fe(CN)_6]^{4-/3-}$) solution. Cyclic voltammograms (CV) were recorded from −1 to 1 V *vs* Ag/AgCl at a scan rate of 25 mV s^{-1}. The Nyquist plots were recorded at applied potential of 0.09 V *vs* Ag/AgCl, with a frequency range from 10 KHz to 1 Hz. Differential pulse voltammetry (DPV) measurements were carried out with applied potential range of 200 – 700 mV, pulse amplitude 60 mV, pulse period 200 ms, pulse width 100 ms and scan rate of 50 mV/s. The electrochemical measurements were conducted at least in triplicates using a 263A potentiostat/galvanostat equipped with a frequency response detector (FRD100) (Princeton Applied Research Co., Oak Ridge, TN, USA).

Applicability of the immunosensor for real sample analysis

Urine samples were gathered from a healthful person and spiked with various concentrations of AMN from 0.01 to 1 ng mL^{-1} after the negative AMN content verified using LC-MS. Informed consent was obtained from the participant enrolled in this study. The sample collection and analysis steps followed the IRB-approved protocol (Faculty of Medicine Ethical Committee- Alexandria University, IRB approval No: 00012098) and followed the principles outlined in the Declaration of Helsinki for all human experimental investigations. Prior the direct analysis using the developed immunosensor, the urine samples were diluted 2 times with PBS buffer pH 7.2.

Results and discussion

Physico-Chemical characterizations of the produced Cel NFMs

First, cellulose nanofibers were created from cellulose acetate nanofibers using a regeneration approach (Fig. 1A). The successful conversion of acetate group of Cel-A to hydroxyl groups of cellulose was proofed using Fourier-transform infrared spectroscopy (FT-IR). Figure 1B presents the FT-IR spectra of the Cel NFM (curve b) and the pristine Cel-A NFM (curve a). After the regeneration process, the peak at around 1750 cm^{-1} ascribed to C=O of the ester of Cel-A disappeared and a new distinctive peak at about 3450 cm^{-1} corresponded to the stretching vibration of -OH appeared (Figure 1B), suggesting that acetate was successfully converted to hydroxyl groups.

The decoration of the cellulose nanofibrous membranes with citric acid was carries out as shown in Fig. 1C. The appeared peak of C=O of the ester at 1750 cm confirmed the successful grafting of CA onto the NFM and the effective incorporation of carboxyl groups onto the Cel NFM surface between the hydroxyl group of the regenerated cellulose nanofibers and carboxylic acid (-COOH) group of CA, and the decrease of hydroxyl group peak intensity at 1042 cm^{-1} (Fig. 1D)[26,27].

The morphologies of the nanofibrous membranes were characterized by scanning electron microscopy (SEM). SEM images of electrospun Cel-A NFMs in Fig. 2 a and b demonstrated that the Cel-A nanofibers were aligned and assembled with average diameter of 290 nm as a non-woven fabric[28]. The Cel-A nanofibers ester groups were converted through the

deacetylation process to hydroxyl groups, the Cel NFMs still retained the morphology and similar average diameter (Fig. 2 c and d).

Electrochemical impedance spectroscopy and cyclic voltammetry characterization

The effect of using of the nanofibrous membranes as a supporting matrix for the immobilization of the antibodies during the immunosensor fabrication was examined by comparing the electrochemical performance between screen-printed electrodes modified with Cel casted membranes (Cel CM/SPE) and Cel nanofibrous membranes (Cel NFM/SPE). The effective surface area of the different modified electrodes was calculated according to Randles-Sevcik equation[29].

$$i_p = 2.69 \times 10^5 \mathrm{An}^{3/2} \mathrm{D}^{1/2} \mathrm{C} \upsilon^{1/2} \quad [2]$$

where A is effective area of an electrode, n is electrons transferred number, D is the diffusion coefficient, C is electrolyte solution concentration while υ is the scan rate. The Cel CM/SPE had a higher electroactive surface area by about 3 times in comparison with the Cel CM/SPCE (Fig. 3A). The improvement in the electroactive surface of the Cel NFM/SPCE could be due to the unique microporous structure of the nanofibrous membranes which can facilitate easy access of analytes toward the surface of the electrode and accelerate the electron movement between the analyte and the electrode surface, introducing the nanofibers as an ideal matrix for development of highly sensitive sensing platforms.

Electrochemical impedance spectroscopy (EIS) is an effective technique for probing the features of surface-modified electrodes made through the fabrication process. Impedance spectra consist of two parts: a semicircle portion that corresponds to the electron-transfer-resistance (R_{et}), and a linear portion which reflects the diffusion process[30]. Fig. 3B shows the Nyquist plots observed after modification of the SPE surface with Cel NFM with different nanofibrous membranes thicknesses of 0.05, 0.1 and 0.2 mm. It was shown that R_{et} was directly proportional to nanofibrous membrane thickness. Due to its lower insulating effect, a membrane thickness of 0.05 mm was found to be most suitable for further experiments.

Cyclic voltammograms were recorded with the developed immunosensor between −1 and 1 V vs Ag/AgCl in PBS pH 7.2. No oxidation nor reduction peak was observed in the absence of AMN. After incubation of the immunosensor with AMN at concentration of 1 μg mL^{-1}, one anodic peak appeared at approximately 0.45 V, and a cathodic peak was observed at −0.05 V (Fig. 3C). The anodic peak could be attributed to the electrochemical oxidation of AMN hydroxyindole to quinone imine with two electrons and two protons. Based on these results, a potential of 0.45 V vs Ag/AgCl was selected for AMN immunosensing.

Optimization of the experimental conditions for AMN detection

The analytical performance of the fabricated immunosensor were adjusted by optimizing different parameters including antibodies concentration, tethering time of antibodies, temperature and immunoreaction time and the pH value of the electrolyte solution.

Anti-AMN antibodies concentration—The influence of antibody concentration on the sensor response to AMN (1 ng mL^{-1}) was examined using the Cel NFM-modified SPE activated using 1mM EDC/NHS and an immobilization time of 60 min. The current response steadily increased as antibody loading increased. The highest amperometric signal was achieved by using of anti-AMN antibodies at concentration of 100 μg mL^{-1}. However, the sensor response was diminished at antibody concentrations greater than 150 μg mL^{-1} (Fig. 4a). This could be because of steric hindrance of the antibodies, which may influence accessibility of the AMN molecules to the binding sites of the antibodies on the nanofibrous membranes[31]. As a result, the ideal anti-AMN antibodies concentration for the immunosensor fabrication was determined to be 100 μg mL^{-1}.

Antibodies immobilization time—By using the antibody immobilization procedure with antibodies concentration of 100 g mL^{-1} at 4°C for various durations ranging from 10 to 120 min, the impact of antibodies immobilization time on the immunosensor response was investigated. The immunosensor response to AMN (1 ng mL^{-1}) increased with raising the time of antibodies tethering up to 60 min Fig. 4b. Nonetheless, longer incubation periods did not result in higher amperometric signals, indicating that active sites on the nanofibrous membrane were saturated. Further experiments were carried out by using immobilization time of 60 minutes.

Immunoreaction temperature—The AMN reaction with immobilized antibodies is significantly influenced by the incubation temperature, which also affects the obtained current. The response signal was observed to raise with increasing the temperature and reach a maximum value at 37 °C (Fig. 4c). Thereafter, the signal progressively diminishes, most likely as a result of the denaturation of the immobilized antibodies[32]. Therefore, 37°C was chosen as the ideal temperature for the formation of immunocomplexes.

Immunoreaction time—The immunosensor response to AMN at the concentration of 1 ng mL^{-1} was assessed after incubation durations varying from 5 to 60 minutes. Fig. 4d clearly indicates that the immunosensor response raised linearly with incubation time and reaches a plateau after 30 minutes, showing that the AMN molecules fully interacted with the immobilized antibodies[32].

pH of the electrolyte solution—The pH of the electrolyte solution is an important element in the performance evaluation of an immunosensor. Fig. 4e depicts the influence of PBS pH values ranging from 5 to 8.5 on the current response of the fabricated immunosensor. The experimental results demonstrated that the immunosensor response increases as the pH value increases from 5 to 7.2, and subsequently decreases as the pH value increases from 7.2 to 8.5. The reasons for this are most likely related to the biological activity of the antibody, which decreased in acid and alkaline solutions, and the antigen-antibody complex might readily disintegrate in the inappropriate pH of the working solution[33,34].

Detection of amanitin

With optimizing the different experimental factors, the analytical performance of the developed immunosensor for AMN detection was investigated at different concentrations. A 100 μl of the sample was added to the immunosensor surface and incubated at 37 °C for 30 min. After the immunosensor washing with PBS buffer pH 7.2 to remove non-binded AMN, the electrochemical measurements were carried out using PBS buffer (pH 7.2) as electrolyte. Figure 5A depicts the DPV responses of the fabricated immunosensor at different concentration levels of AMN, it was obvious that the achieved current increased as AMN concentration increased. As observed in Figure 5B, the current responses exhibited a linear increase with the logarithm of AMN concentration in the range of 9 pg mL^{-1} to 2 ng mL^{-1} (R^2=0.9901). The developed immunosensor showed a high sensitivity toward AMN with a limit of detection (LOD) at 8.3 pg mL^{-1} (LOD=$3S_b$/m, where S_b is the standard deviation of the blank and m is the slope of the calibration plot.). The designed immunosensor performed good in terms of LOD and detection range, but its key benefit is that direct detection of AMN and does not require any extra reagent. It is not based on time-consuming and expensive AMN-conjugates-based competitive approaches. when comparing the fabricated electrochemical immunosensor to other AMN detection biosensors (Table 1), the developed nanofibers-based electrochemical immunosensor observed a good behavior in terms of LOD and linear range with a main advantage is related to the fact that detection of AMN is direct and does not involve any additional reagent. Moreover, the ultrahigh sensitivity of the nanofibers-based electrochemical immunosensor could be attributed to including the microporous nanofibrous membranes enhancing the accessibility of the AMN to the recognition sites and accelerating the electron transfer, consequently improving the sensing surface.

Immunosensor specificity, reusability, and stability

One of the main challenges in the field of sensing technology is developing a sensor to selectively identify the desired target in samples comprising multiple closely related compounds. The specificity of the fabricated immunosensor was studied by analyzing 0.1 ng mL^{-1} of mushroom toxins including psilocybin, muscimol, and ibotenic acid as well as cyclic peptides including microcystin-LR and nodularin. Cross reactivity (CR%) was investigated by calculating the reaction to each antibiotic in terms of AMN-equivalent concentration using the AMN calibration curve, it was presented as a percentage of AMN response[43]. As shown in Table S1, the developed immunosensor was highly specific toward AMN as there was no cross-reactivity with all tested compounds.

The ability of the fabricated immunosensor to be reused may help to lower the cost of medical screening tests and minimize medical waste. After detecting 0.1 ng mL^{-1} of AMN, the fabricated immunosensor was regenerate by dipping in 0.1M of glycine hydrochloric acid buffer at pH value of 2.8 for 5 min. As shown in Fig. S1, the developed immunosensor demonstrated good reusability by retaining more than 95% of its original activity after 4 assay cycles and around 88% after the fifth cycle. The loss of activity might be brought either by denaturation of the immobilized antibodies or destruction of the nanofibrous membranes during the repeated regeneration in an acidic glycine buffer[34].

To investigate the stability, the immunosensor was kept at 4°C and its performance was checked every week. After six weeks, the fabricated immunosensor demonstrated still good stability with retaining more than 91% of its initial activity.

Applicability of the developed immunosensor

To validate the feasibility of the fabricated immunosensor in the detection of AMN at low concentrations in real samples, human urine samples were spiked with known concentrations of AMN ranging from 0.01 to 1 ng mL^{-1}. Prior to spiking, the urine samples were analyzed using LC-MS to confirm the free content of AMN. The spiked urine samples were diluted 2 times with PBS without any further treatment before being examined blindly by the developed immunosensor. Each concentration was tested in triplicate. As shown in Table 2, the recovery rate ranged from 92.9% to around 98.7%, with a relative standard deviation (RSD%) of about 4.8%. In addition to the DPV responses of the fabricated immunosensor to different spiked urine samples (Fig. S2), These aforementioned findings demonstrate the applicability, accuracy, and repeatability of the fabricated immunosensor for rapid detection of AMN in the human urine at extremely lower concentration without pre-cleaning for the samples.

Conclusion

An ultrasensitive, disposable, and rapid label-free electrochemical immunosensor for AMN determination was successfully fabricated by using SPEs laminated with a layer of cellulose nanofibrous membranes. The unique structure of cellulose nanofibrous membranes improved the immunosensor response by about 3 times. The immunosensor showed very competitive analytical performances with a LOD value of AMN at 8.3 pg mL^{-1}, as well as stability over time. Furthermore, the feasibility of using the immunosensor in accurate determination of AMN in human urine samples without any pretreatment has been demonstrated with good recovery during around 30 min.

Supplementary Material

Refer to Web version on PubMed Central for supplementary material.

Acknowledgment

The research was partially supported by both National Institute of Environmental Health Sciences (NIEHS) (Grant No. 5P42ES004699) and USDA National Institute of Food and Agriculture (USDA-NIFA) program (Grant No. 2015-68003-23411)

References

1. Gummin DD, Mowry JB, Spyker DA, Brooks DE, Osterthaler KM and Banner W, Clin Toxicol, 2018, 56, 1213–1415.
2. Brandenburg WE and Ward KJ, Mycologia, 2018, 110, 637–641. [PubMed: 30062915]
3. Cervellin G, Comelli I, Rastelli G, Sanchis-Gomar F, Negri F, De Luca C and Lippi G, Hum Exp Toxicol, 2018, 37, 697–703. [PubMed: 28905663]
4. Graeme KA, Journal of Medical Toxicology, 2014, 10, 173–189. [PubMed: 24573533]
5. Durand FC and Valla D, Drug-Induced Liver Disease, 2013, 621–629.

6. Taylor SL, Encyclopedia of Food Sciences and Nutrition, 2003, 5813–5819.
7. Bever CS, Swanson KD, Hamelin EI, Filigenzi M, Poppenga RH, Kaae J, Cheng LW and Stanker LH, Toxins (Basel), 2020, 12, 123. [PubMed: 32075251]
8. Bambauer TP, Wagmann L, Weber AA and Meyer MR, Toxins (Basel), 2020, 12, 1–14.
9. Varvenne D, Retornaz K, Metge P, De Haro L and Minodier P, Pediatr Emerg Care, 2015, 31, 277–278. [PubMed: 25831030]
10. Enjalbert F, Rapior S, Nouguier-Soulé J, Guillon S, Amouroux N and Cabot C, J Toxicol Clin Toxicol, 2002, 40, 715–757. [PubMed: 12475187]
11. Chen C, Zhao X-L, Li Z-H, Zhu Z-G, Qian S-H and Flewitt A, Sensors, 2017, 17, 182. [PubMed: 28106820]
12. Lopez GA, Estevez M-C, Soler M and Lechuga LM, Nanophotonics, 2017, 6, 123–136.
13. El-Moghazy AY, Wisuthiphaet N, Yang X, Sun G and Nitin N, Food Control, 2022, 135, 108811.
14. El-Moghazy A, Amaly N and Sun G, in 29th Annual UC Davis Biotechnology Program Retreat, 29th Annual UC Davis Biotechnology Program Retreat, Davis, 2023.
15. El-Moghazy A, Amaly N and Sun G, 2021, 8179.
16. Quirós J, Boltes K and Rosal R, Polymer Reviews, 2016, 56, 631–667.
17. Ray SS, Chen S-S, Li C-W, Nguyen NC and Nguyen HT, RSC Adv, 2016, 6, 85495–85514.
18. Lu X, Wang C, Favier F and Pinna N, Adv Energy Mater, 2017, 7, 1601301.
19. Amaly N, Pandey P, EL-Moghazy AY, Sun G and Pandey PK, Talanta, 2022, 242, 123281. [PubMed: 35180535]
20. Amaly N, EL-Moghazy AY, Sun G and Pandey P, J Environ Manage, DOI:10.1016/j.jenvman.2020.111574.
21. El-Moghazy AY, Amaly N, Istamboulie G, Nitin N and Sun G, Microchimica Acta, 2020, 187, 535. [PubMed: 32870397]
22. El-Moghazy AY, Huo J, Amaly N, Vasylieva N, Hammock BD and Sun G, ACS Appl Mater Interfaces, 2020, 12, 6159–6168. [PubMed: 31927905]
23. Fu Q, Si Y, Duan C, Yan Z, Liu L, Yu J and Ding B, Adv Funct Mater, 2019, 29, 1–11.
24. H. Y. Liu H , J Polym Sci—Polym Phys, 2002, 40, 2119–2129.
25. Amaly N, Si Y, Chen Y, El-Moghazy AY, Zhao C, Zhang R and Sun G, Colloids Surf B Biointerfaces, 2018, 170, 588–595. [PubMed: 29975907]
26. Cerroni B, Cicconi R, Oddo L, Scimeca M, Bonfiglio R, Bernardini R, Palmieri G, Domenici F, Bonanno E, Mattei M and Paradossi G, Heliyon, 2018, 4, e00770. [PubMed: 30238062]
27. Fu Q, Wang X, Si Y, Liu L, Yu J and Ding B, ACS Appl Mater Interfaces, 2016, 8, 11819–11829. [PubMed: 27111287]
28. Ding SSB, Li C, Fujita S, Colloid. Surface. A, 2006, 285, 257–262.
29. Randles JEB, Transactions of the Faraday Society, 1948, 44, 322–327.
30. Santaclara FJ, Pérez-Martín RI and Sotelo CG, Food Chem, 2014, 143, 22–26. [PubMed: 24054207]
31. Qiao L, Wang X and Sun X, Int J Electrochem Sci, 2014, 9, 1399–1414.
32. Zhang N, Xiao F, Bai J, Lai Y, Hou J, Xian Y and Jin L, Talanta, 2011, 87, 100–105. [PubMed: 22099655]
33. Yang Y, Liu Q, Liu Y, Cui J, Liu H, Wang P, Li Y, Chen L, Zhao Z and Dong Y, Biosens Bioelectron, 2017, 90, 31–38. [PubMed: 27871047]
34. Li F, Han J, Jiang L, Wang Y, Li Y, Dong Y and Wei Q, Biosens Bioelectron, 2015, 68, 626–632. [PubMed: 25656779]
35. Gao J, Liu N, Zhang X, Yang E, Song Y, Zhang J and Han Q, Molecules, DOI:10.3390/molecules27020538.
36. Bever CS, Swanson KD, Hamelin EI, Filigenzi M, Poppenga RH, Kaae J, Cheng LW and Stanker LH, Toxins (Basel), DOI:10.3390/toxins12020123.
37. He K, Mao Q, Zang X, Zhang Y, Li H and Zhang D, Biologicals, 2017, 49, 57–61. [PubMed: 28688778]

38. Zhou S, Guo L, Xu X, Song S, Liu L, Kuang H, Zhu Y, Xu L and Xu C, Food Chem, DOI:10.1016/j.foodchem.2022.133660.
39. Tian R, Ye Y, Lu X, Sun J, Wang W and Sun X, Highly Sensitive Fluorescent Aptasensor for Detecting α−2 amatoxin Based on Rolling Circle Amplification Triggered by Aptamer-Tetrahedral, 2023.
40. Liu H, Qin Y, Xing W and Ma L, Science and Technology of Food Industry, 2022, 43, 294–301.
41. Bever CS, Adams CA, Hnasko RM, Cheng LW and Stanker LH, PLoS One, DOI:10.1371/journal.pone.0231781.
42. He K, Zhang X, Zhao R, Wang L, Feng T and Wei D, Microchimica Acta, 2016, 183, 2211–2219.
43. Gaudin V and Maris P, Food Agric Immunol, 2010, 37–41.

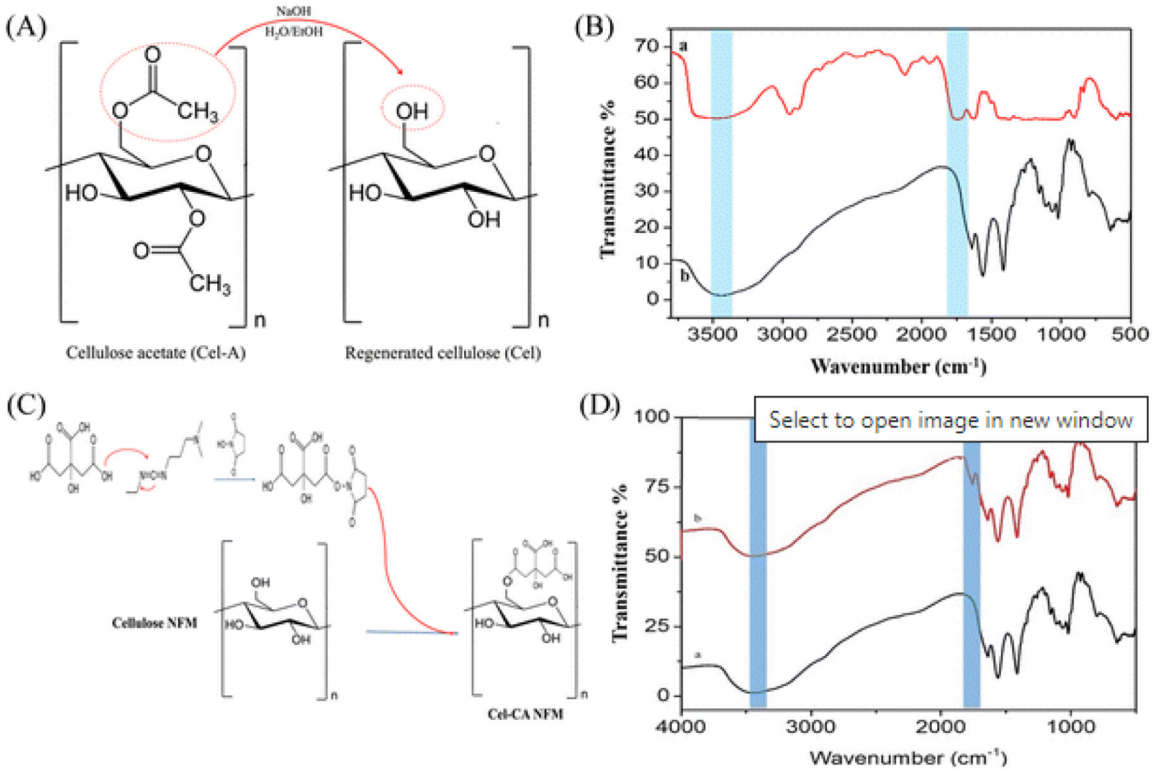

Fig. 1.

(A) Scheme of the deacetylation process of cellulose acetate. (B) FT-IR spectra of (a) Cel-A NFM and (b) regenerated Cel NFM. (C) Scheme of grafting of citric acid onto Cel NFM. (D) FT-IR spectra of (a) Cel NFM and (b) Cel NFM decorated with citric acid.

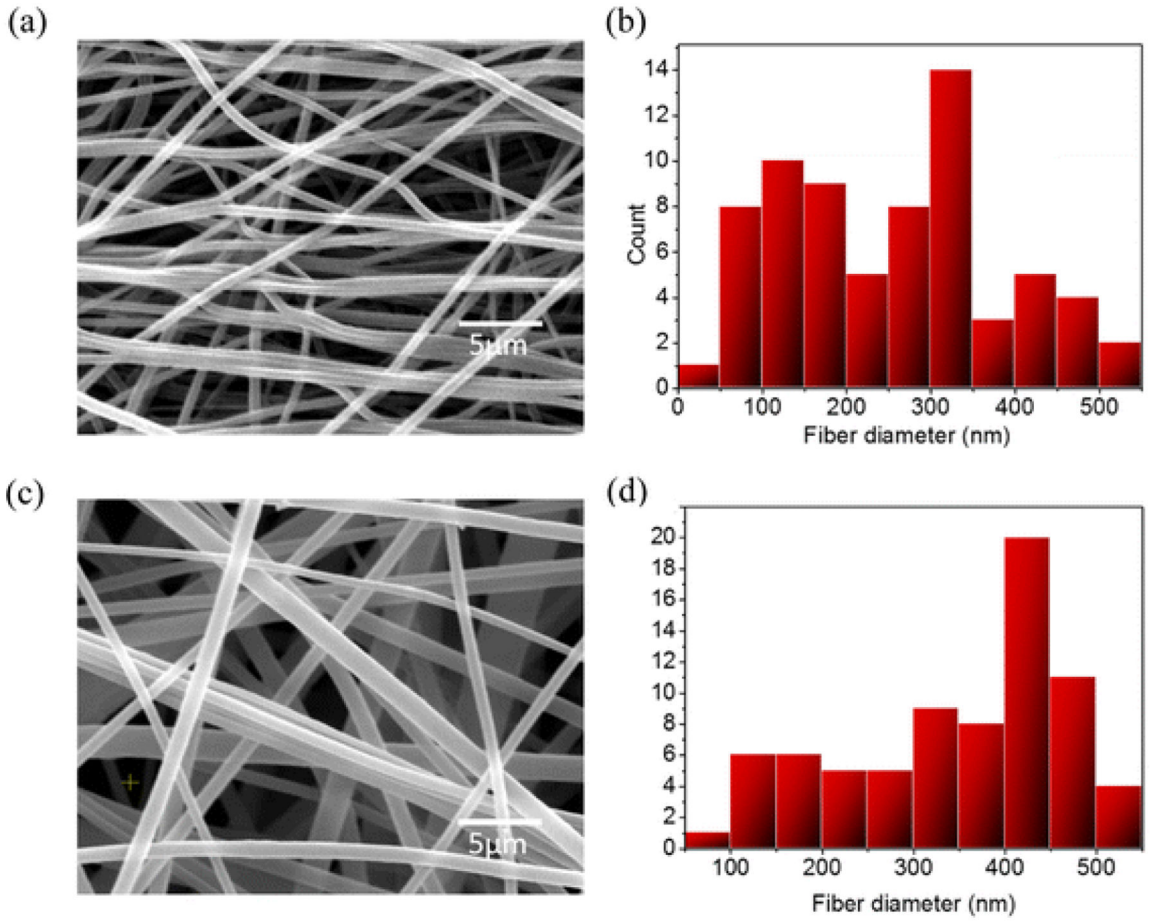

Fig. 2.

(a) SEM image and (b) diameter distribution of cellulose acetate NFM. (c) SEM image and (d) diameter distribution of Cel NFM.

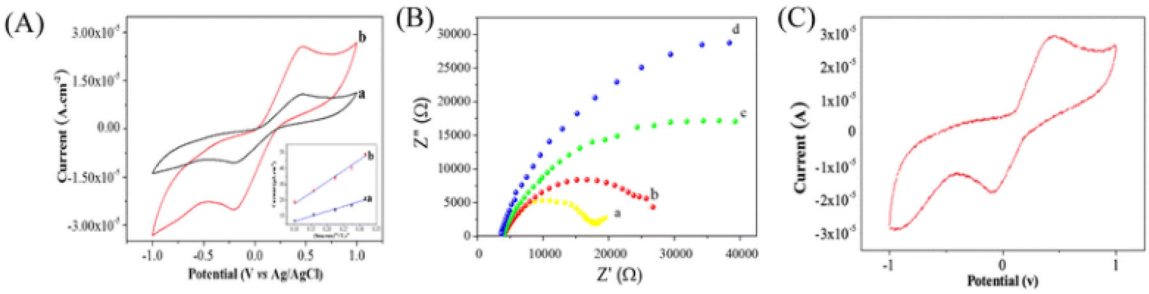

Fig. 3.

(A) CV scans of 2.5 mM [Fe(CN)6]3−/4− at a scan rate of 25 mV s−1 for (a) Cel CM/SPE and (b) Cel NFM/SPE. (B) EIS Nyquist plots in 2.5 mM [Fe(CN)6]4−/3− for (a) bare SPE, (b) Cel NFM (0.05 mm)/SPE, (c) Cel NFM (0.1 mm)/SPE, and (d) Cel NFM (0.2 mm)/SPE. (C) CV scan of AMN (1 μg mL−1) on SPE.

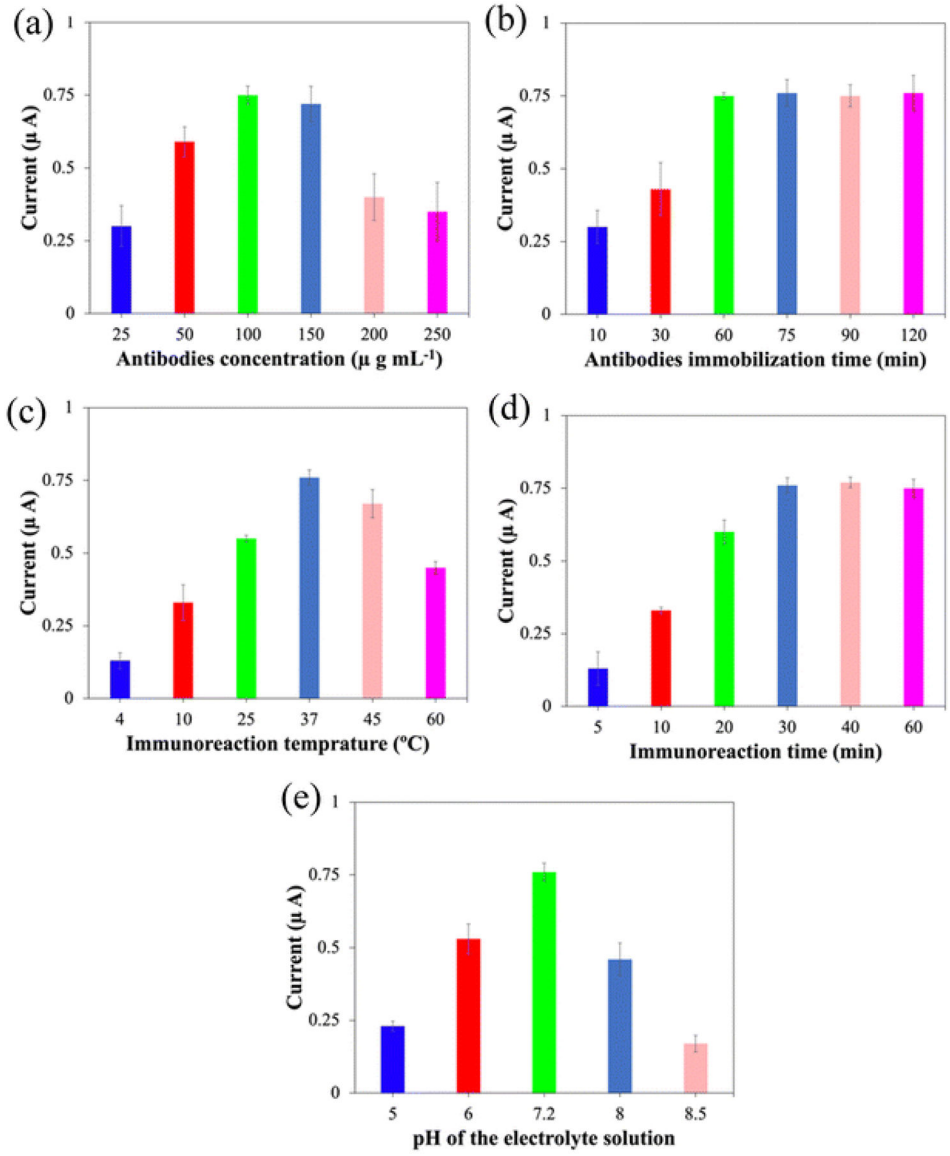

Fig. 4.

Response to 1 ng mL−1 AMN of immunosensors fabricated by using different experimental conditions: (a) antibody concentration, (b) antibody immobilization time, (c) immunoreaction temperature, (d) immunoreaction time, and (e) pH of electrolyte solution.

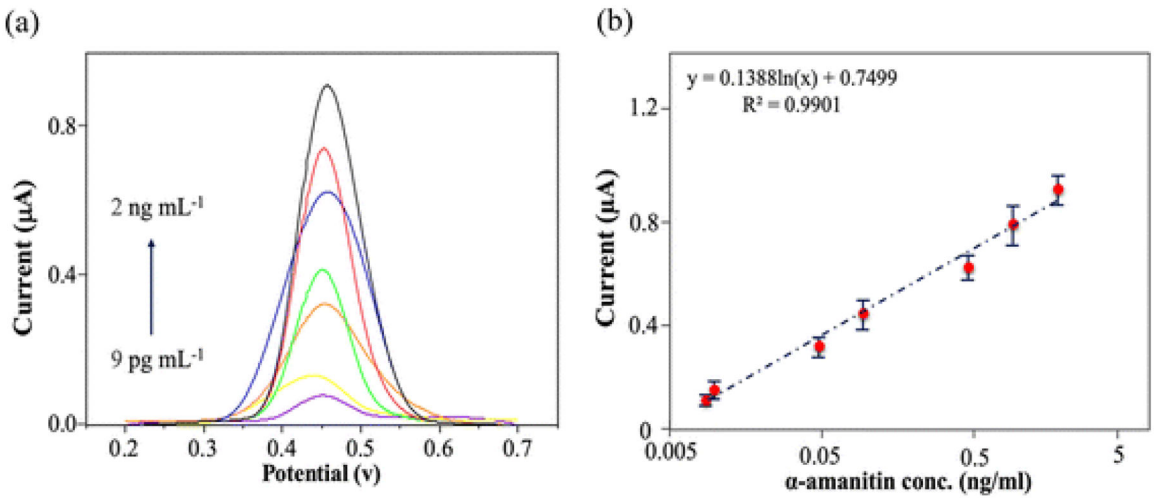

Fig. 5.

(a) Electrocatalytic current responses of the fabricated electrochemical immunosensor for the detection of different concentrations of AMN in the range of 9 pg mL−1 to 2 ng mL−1; (b) calibration curve of the immunosensor for the detection of different concentrations of AMN (n = 3).

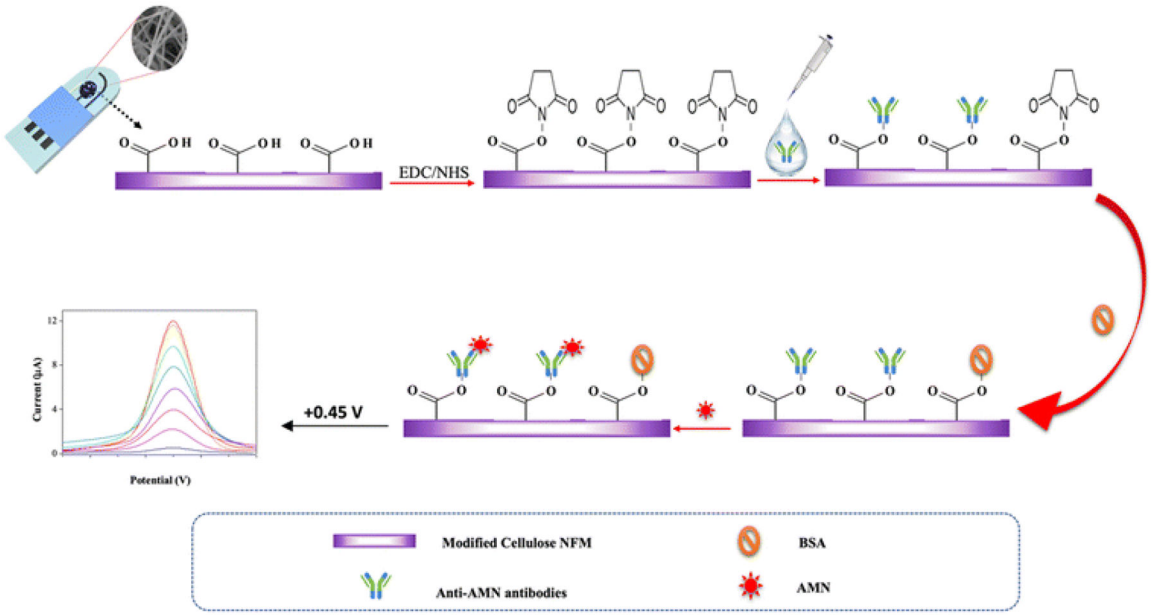

Scheme 1.

Fabrication process and sensing mechanism of the electrochemical immunosensor for AMN detection.

Table 1

Comparison of the detection range and detection limit for AMN of the developed immunosensor with those of other biosensors in previously published studies

Method	Range	LOD	Ref.
ELISA	1–6 μg mL^{-1}	0.1 μg mL^{-1}	35
LFIA	0.3–10 ng mL^{-1}	0.3 ng mL^{-1}	36
ELISA	1–120 ng mL^{-1}	0.91 ng mL^{-1}	37
LFIA	0.1–50 ng g^{-1}	0.1 ng g^{-1}	38
Fluorescent aptasensor	0.01–5 μg mL^{-1}	7 ng mL^{-1}	39
ELISA	1.18–15.00 ng mL^{-1}	0.88 ng mL^{-1}	40
LFIA	0.3–10 ng mL^{-1}	0.3 ng mL^{-1}	41
Gold-nanoparticle based immunochromatographic	2 ng/mL^{-1}-2 μg mL^{-1}	1.9 ng mL^{-1}	42
Electrochemical immunosensor	0.009–2 ng mL^{-1}	8.3 pg mL^{-1}	This work

Table 2

Recoveries of AMN from spiked human urine samples determined using the immunosensor.

Sample	Spiked concentration (ng mL^{-1})	Found concentration (ng mL^{-1})	Recovery (%)
1	0	ND	—
2	0.01	0.0093	92.9
3	0.05	0.0481	96.2
4	0.1	0.0943	94.3
5	1	0.987	98.7